The eddy current probe array for Keda Torus eXperiment

Zichao Li, Hong Li, Cui Tu, Jintong Hu, Wei You, Bing Luo, Mingsheng Tan, Yolbarsop Adil, Yanqi Wu, Biao Shen, Bingjia Xiao, Ping Zhang, Wenzhe Mao, Hai Wang, Xiaohui Wen, Haiyang Zhou, Jinlin Xie, Tao Lan, Adi Liu, Weixing Ding, Chijin Xiao, and Wandong Liu

Citation: Review of Scientific Instruments **87**, 113503 (2016); doi: 10.1063/1.4966988
View online: http://dx.doi.org/10.1063/1.4966988
View Table of Contents: http://aip.scitation.org/toc/rsi/87/11
Published by the American Institute of Physics

The eddy current probe array for Keda Torus eXperiment

Zichao Li,[1] Hong Li,[1,a)] Cui Tu,[1] Jintong Hu,[1] Wei You,[1] Bing Luo,[1] Mingsheng Tan,[1] Yolbarsop Adil,[1] Yanqi Wu,[1] Biao Shen,[2] Bingjia Xiao,[2] Ping Zhang,[2] Wenzhe Mao,[1] Hai Wang,[1] Xiaohui Wen,[1] Haiyang Zhou,[1] Jinlin Xie,[1] Tao Lan,[1] Adi Liu,[1] Weixing Ding,[1,3] Chijin Xiao,[1,4] and Wandong Liu[1]

[1]*CAS Key Laboratory of Geospace Environment, Department of Modern Physics, University of Science and Technology of China, Hefei 230026, People's Republic of China*
[2]*Institute of Plasma Physics, Chinese Academy of Sciences, Hefei 230031, People's Republic of China*
[3]*Department of Physics and Astronomy, University of California, Los Angeles, California 90095, USA*
[4]*Plasma Physics Laboratory, University of Saskatchewan, Saskatoon, Saskatchewan 7N 5E2, Canada*

(Received 30 July 2016; accepted 22 October 2016; published online 8 November 2016)

In a reversed field pinch device, the conductive shell is placed as close as possible to the plasma so as to balance the plasma during discharge. Plasma instabilities such as the resistive wall mode and certain tearing modes, which restrain the plasma high parameter operation, respond closely with conditions in the wall, in essence the eddy current present. Also, the effect of eddy currents induced by the external coils cannot be ignored when active control is applied to control instabilities. One diagnostic tool, an eddy current probe array, detects the eddy current in the composite shell. Magnetic probes measuring differences between the inner and outer magnetic fields enable estimates of the amplitude and angle of these eddy currents. Along with measurements of currents through the copper bolts connecting the poloidal shield copper shells, we can obtain the eddy currents over the entire shell. Magnetic field and eddy current resolutions approach 2 G and 6 A, respectively. Additionally, the vortex electric field can be obtained by eddy current probes. As the conductivity of the composite shell is high, the eddy current probe array is very sensitive to the electric field and has a resolution of 0.2 mV/cm. In a bench test experiment using a 1/4 vacuum vessel, measurements of the induced eddy currents are compared with simulation results based on a 3D electromagnetic model. The preliminary data of the eddy currents have been detected during discharges in a Keda Torus eXperiment device. The typical value of toroidal and poloidal eddy currents across the magnetic probe coverage rectangular area could reach 3.0 kA and 1.3 kA, respectively. *Published by AIP Publishing.* [http://dx.doi.org/10.1063/1.4966988]

I. INTRODUCTION

To maintain plasma equilibrium in fusion devices, and especially in reversed field pinch (RFP) devices, not only is the good magnetic field configuration formed by the external coil discharge vital but also the conductive shell. If the inside or outside magnetic field penetrates through the shell, the eddy current induced in the shell will oppose its presence and rebuild the magnetic field configuration. Indeed, in a RFP device, the magnetic surfaces are constructed by electric currents flowing through the external coils, the conductive shell, and the plasma itself.

Positioning the conductive shell as close as possible to the plasma helps in restraining the rapid growth of plasma instabilities such as the resistive wall mode and tearing mode. The presence of a shell will stabilize the external kink mode because of induced eddy currents that oppose the growth of the perturbation. Bondeson and Ward[1] showed that if the plasma is rotating sufficiently fast relative to the wall, low-n external modes can be stabilized by image currents in the resistive walls leading to notable increases in the beta limit. A wall with finite conductivity can destabilize the resistive tearing modes, but these instabilities can be stabilized through sufficiently fast plasma rotation. Eddy currents in the resistive wall, driven by rotating magneto-hydro-dynamic (MHD) activity, will produce a non-linear torque to slow down the plasma rotation. The shell's significant role makes this effect especially strong in RFP devices and leads to shorter mode-lock times than in the tokamak.[2]

Also, the effect of eddy currents induced by the external coils cannot be ignored when active control is applied to control instabilities. Not only eddy currents in the resistive shell but also external error fields contribute to slow down the rotation of the tearing mode.[3]

Moreover, the conductive shell surrounding the plasma usually is not completely continuous and has a complex three-dimensional geometry resulting in a more complicated eddy current distribution. From in-depth research of the plasma instabilities and perturbations, taking the three-dimensional details of the conducting structures into account is becoming more and more important. Villone *et al.*[4] combined the plasma response matrix with the 3D volumetric integral formulation of the eddy current problem and demonstrated that the 3D effect of the gaps can lead to a significant increase in the growth rate of the resistive wall mode.

The eddy current in the vacuum vessel is usually measured by the electromagnetic measurements, such as flux loops, magnetic probes, or a flexible printed circuit board with magnetic

a)honglee@ustc.edu.cn

probes and other magnetics.[5–8] Obtaining the eddy current is useful to correct the measurement of plasma current or to research the interaction between the plasma and the wall during plasma disruption. As far as we know, no one probe array can measure both the toroidal and the poloidal components of eddy currents at the entire shell simultaneously.

Electromagnetic measurements are a fundamental diagnostic system to identify plasma equilibrium, MHD instabilities, plasma disruptions, and self-organization phenomenon in a tokamak or other magnetic confined devices.[9–12] Magnetic probes with a bandwidth about 1.1 MHz are developed to measure high-frequency instabilities in DIII-D.[13] A movable magnetic probe system installed in the T-10 tokamak allowed the identification of the fast-scale magnetic oscillations during the plasma disruption with high density.[14] Anisotropic magnetic turbulences are observed by high-frequency magnetic probes whose bandwidth can reach 2.5 MHz in MST.[15] The eddy current probe array (ECPA) in a new RFP device Keda Torus eXperiment (KTX)[16] introduced in this paper extends the application of electromagnetic measurements to detect the eddy current in the shell and vortex electric field, providing the boundary information in detail.

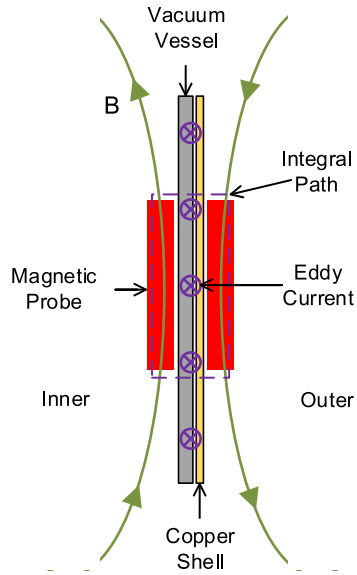

FIG. 1. Schematic of the eddy current measurement by magnetic probes. The current flowing into the rectangular area could be obtained by integrating the magnetic field along the closed path.

II. PRINCIPLE OF MEASUREMENT AND KTX COMPOSITE STRUCTURE

A. Principle of measurement

The current density can be worked out by the differential measurement of two magnetic probes of uniform size but located on either side of the current sheet. The working principle of the eddy current probe on the conductive shell (Fig. 1) is based on the Ampere's circuital law. The current flowing across the rectangular area can be obtained by integrating the magnetic field along the closed path. Provided that the normal magnetic field near the shell is much less than the tangential component and the sum of magnetic probe spacing and thickness is less than that of its width, the integral along the short side can be ignored. The current is then simplified,

$$\oint \mathbf{B} \cdot dl \approx L(B_{outer} - B_{inner}) = \mu_0 I \qquad (1)$$

which suggests that the eddy current in the shell can be derived easily by the magnetic probes from the difference between the inner and outer magnetic fields.

B. KTX composite structure

KTX is a medium-sized RFP device with major radius $R = 1.4$ m and minor radius $a = 0.4$ m. Its composite shell is designed for mechanical support, plasma control, and MHD instability suppression.[17] The composite shell in KTX includes a 6-mm stainless steel vacuum chamber and a 1.5-mm copper shell. The copper shell consists of three different sections: one primary copper shell, two poloidal shield shells, and two toroidal shield shells.[18] As the diagnostics of eddy currents depends on the structural feature of the shell, the copper shell is described in detail.

(1) The primary copper shell: The inner part is a 1.5-mm copper shell with a penetration time of 20 ms and a 1.5-mm layer of polytetrafluoroethylene (PTFE) is filled between the vacuum chamber and the primary copper shell. Two insulated poloidal gaps and one equatorial toroidal gap on the high field side (HFS) are incorporated into the primary copper shell. There are also two insulated poloidal gaps in the vacuum chamber at the same position as well as the primary copper shell.

(2) The poloidal shield shells: The eddy current induced by the plasma in the primary shell changes flow direction at the poloidal and toroidal gaps, leading to large error fields and deforming the shape of equilibrium surface. Two poloidal shield shells are set at two poloidal gaps outside the primary shell. Each poloidal shield shell is designed to be detachable and electrically connected by 16 copper bolts. The poloidal shield shell spans 50° along the toroidal direction.

(3) The toroidal shield shells: Two toroidal shield shells are set at two toroidal gaps outside the primary shell. The toroidal shield shell spans 60° along the poloidal direction.

The composite shell in KTX is optimally designed from the beginning to be able to measure eddy currents. It meets three criteria based on principle of measurement as follows: (A) Its thickness (9 mm) is less than the width of the magnetic probe (L = 40 mm). (B) The normal magnetic field near the shell is weak resulting from choosing the good conductor as the shell. (C) The conductive current in the shell is much larger than the displacement current. Because the conductivity of the copper shell and vacuum vessel is 5.7×10^7 S/m and 1.4×10^6 S/m, respectively, the vortex electric field could drive as large as 3 kA/cm^2 conductive current in the shell.

III. EDDY CURRENT PROBE ARRAY

A. Probe array system

The eddy current probe array consists of two parts: 320 two-dimension magnetic probes located on the inner and outer

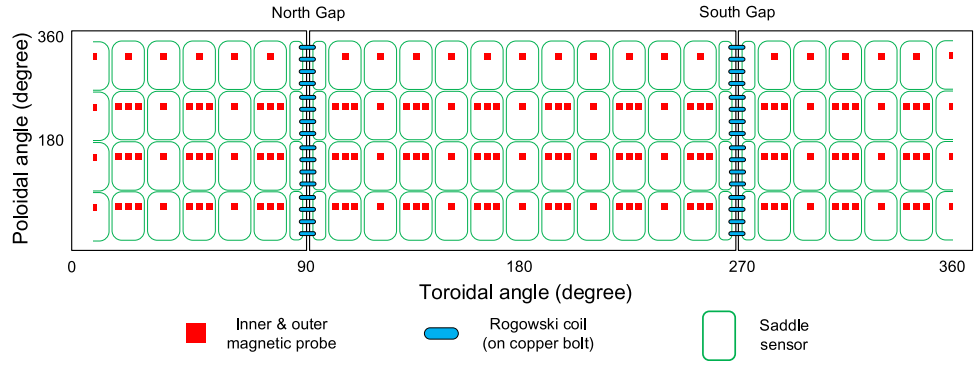

FIG. 2. Distribution of eddy current probe array in Keda Torus eXperiment. The black rectangles represent the composite shell. The inner and outer magnetic probes are located inner the vacuum vessel and outer the copper shell.

sides of the KTX composite shell and 32 Rogowski coils located at the two poloidal gaps (Fig. 2). The 46 sets of 2D magnetic probes (for measuring the toroidal and poloidal magnetic fields) are located unevenly along the toroidal direction on the inner surface of the vacuum vessel (VV). The shorter spacing between the two probes along the toroidal direction is 8.4 cm. In total, four poloidal arrays of magnetic probes are placed in the VV, with the exception of the HFS, where only 22 sets of probes are placed every 15° in the toroidal direction because of space limitations. Identical magnetic probes are located outside the shell at the same positions and well aligned with the inner probes. All probes are placed close to the surface of the composite shell. Magnetic field fluctuations with spatial poloidal wave number in the range $|m| \leq 2$ and toroidal components in the range $|n| \leq 24$ can be measured. The resolution of the magnetic probes is 2 G at 1 kHz and the frequency response is at least within 200 kHz. The real products of the probes (Fig. 3) and details of their parameter values are listed in Table I.

The parameter values of the magnetic probes were selected in consideration of the internal environment of the KTX VV, i.e., the maximum magnetic field 1 T, the largest plasma current 1 MA, and the highest baking temperature 300 °C. Sintered ceramic is chosen as the core of the magnetic probe, for which the 3D size is 40 mm × 40 mm × 11 mm, and the coil wire is a 0.7 mm PTFE line. The two individual coils are perpendicular to each other to measure the toroidal and poloidal fields.

The 16 Rogowski coils located at each gap measure the currents through the copper bolts. These bolts are located outside the VV where the temperature is relatively low. Polyurethane plastic of diameter 4 mm and length 11 cm is chosen for the core of the Rogowski coil; the coil wire is made of PTFE. The Rogowski coils in conjunction with the 2D magnetic probes are able to provide the distribution of the eddy current over the entire composite shell.

B. Calibration of probes

The measurement principle of magnetic probe is based on Faraday's law. In a magnetic field B(t) varying with time, the electromotive force induced on the coil is

$$\varepsilon = -\frac{d\phi}{dt} = -S_{eff}\frac{dB_{\perp}}{dt}, \tag{2}$$

where $B_{\perp}$ is the magnetic field along the axis of coil, and $S_{eff} = NS + \Delta S$ is the effective area with N the number of turns of the coil, S the section area of coil, and ΔS the stray area.

Accurate measurement of the magnetic field requires calibration of each magnetic probe. The secondary calibration method is used whereby the magnetic probe under test and a standard magnetic probe are placed in the same time-varying magnetic field for comparison (Fig. 4). As the time derivative of $B_{\perp}$ is the same, the effective area is obtained by calculating the ratio of the voltages of two probes.

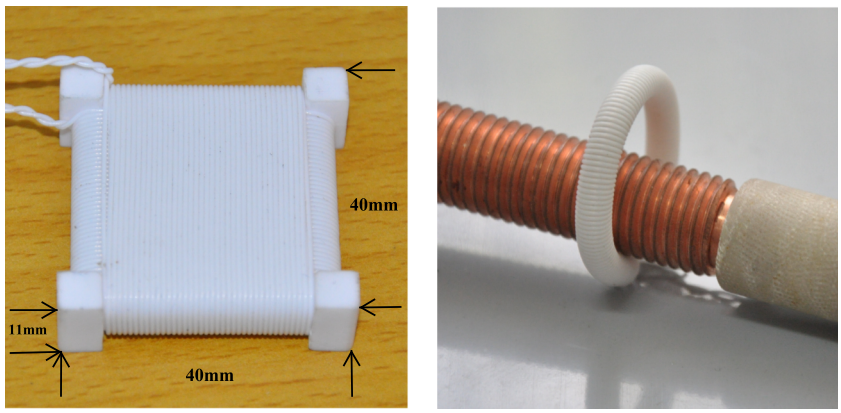

FIG. 3. 2D magnetic probe and the Rogowski coil on copper bolt.

TABLE I. Parameters and their values of the 2D magnetic probe.

Probe	Turns	Effective area (m^2)	Frequency response (kHz)
Poloidal	2×37	0.023	~200
Toroidal	4×37	0.024	~300

A long straight solenoid is powered by a high-speed dual polarity power supply featuring a stable current regulation and a wide dynamic range of ±60 V/±10 A. In the calibration test, the power supply is set to output 1 kHz 3 A_{pp} sine waveforms. In the middle of the solenoid is a platform on which the standard probe and the test probe are symmetrically placed 5 cm away from the center. Near the center of the solenoid, the error of magnetic field along axis is less than 0.16% and the error along the radial direction is less than 0.11%. The standard probe is wound in two layers of enameled wire on a rectangular epoxy resin core of size 88 mm × 50 mm × 35 mm. The effective value of the standard probe is 0.1924 m^2 and the error is less than 0.017%. A non-inductive resistor is inserted in the power circuit and voltages are detected using an acquisition card with a sample frequency: 500 kS/s.

The relative errors of effective value for all the eddy current probes are guaranteed to be less than 0.4% via multiple measurements. The effective values of the 30 Bt probes (Fig. 5) indicate a good uniformity in the probes; each is labeled and recorded when assembled in the KTX to facilitate precision measurements.

In calibrating approximately one thousand KTX probes, the calibration system is simple and effective. The variation in effective values and phases of the 2D magnetic probe over different frequencies is tested (Fig. 6). The frequency responses of the Bp (poloidal field) and Bt (toroidal field) probes were as high as 200 kHz and 300 kHz, respectively. The magnetic probes of KTX are placed in stainless steel boxes to prevent them from plasma bombardment. The frequency responses of the boxed magnetic probes are shown to be free of stainless steel box on the frequency response and phase shift.

To test the Rogowski coils, an electrified coil replaces the solenoid in the calibration system for the magnetic probes. The voltage on the Rogowski coil is

$$\varepsilon = \frac{\mu_0 S N}{l}\frac{dI}{dt} = -M\frac{dI}{dt}, \tag{3}$$

where M and l are the inductance and circumference of the Rogowski coil. As $\varepsilon = -E_0 \cos wt$, hence,

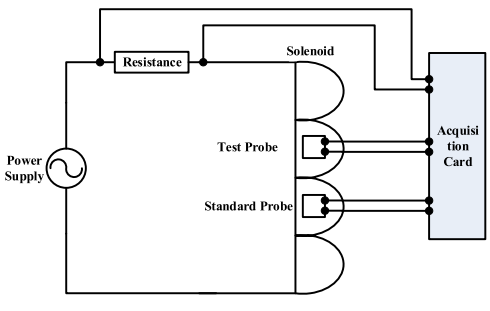

FIG. 4. Schematic of the magnetic probe calibration system.

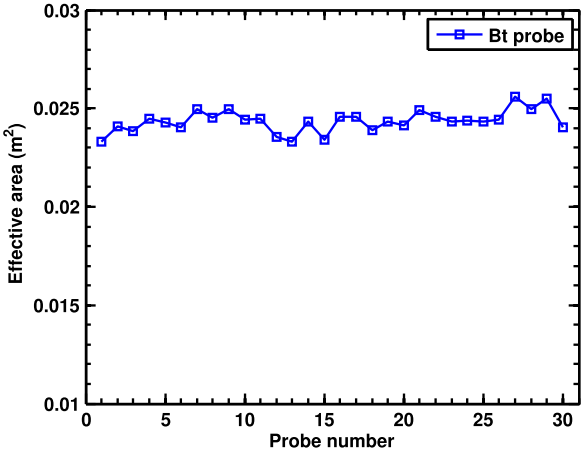

FIG. 5. Effective values of 30 Bt probes by the calibration test.

$$M = \frac{\mu_0 S N}{l} = \frac{E_0}{I_0 w} = \frac{E_0}{2\pi f I_0}. \tag{4}$$

The inductance of the Rogowski coils under different frequencies is close to the theoretical value 2.73×10^{-2} μH. Also, the inductance remains finely stable in the frequency range of interest.

IV. VERIFICATION MODEL AND BENCH TEST OF THE VACUUM VESSEL

Along with the test platform, which includes part of the VV and toroidal field coils, a 3D simulation model with KTX geometric parameters were used to verify the behavior of the ECPA. The inner and outer magnetic fields in the VV were worked out numerically when periodic current waveforms were applied to the toroidal field coil. The difference in the inner and outer magnetic fields along the toroidal direction represented as bell-shaped curves shows maxima at 90° where the toroidal field coil is excited (Fig. 7). The difference in the values of B approaches the eddy current in the shell with decreasing δ. In KTX, the probes are set close to the surfaces of the composite shell, which guarantees that the difference between the magnetic fields is proportional to the eddy current in the shell.

A quarter of vacuum vessel (1/4 VV) whose structural size and materials are identical to the KTX device was used in a bench test experiment and only three toroidal field coils are assembled with it (Fig. 8). Rectangular current waveforms (1 kHz) were applied to the middle toroidal field coil at a duty cycle of 25%. In total 6 (along toroidal axis) × 4 (along poloidal axis) × 2, 2D magnetic probes were embedded in the inner and outer surface of the vessel. The magnetic fields and corresponding eddy current waveforms for one probe are shown in Fig. 9. The eddy current across the magnetic probe coverage rectangular area is calculated by Equation (1) (the width of magnetic probe L = 40 mm) and the minimum resolution of eddy current is 6 A. The current decays exponentially after it peaks and the decay time represents the penetration time of the magnetic field across the VV. The fitted penetration time is 1.3 ms comparable with the theoretically calculated value of 2.0 ms.

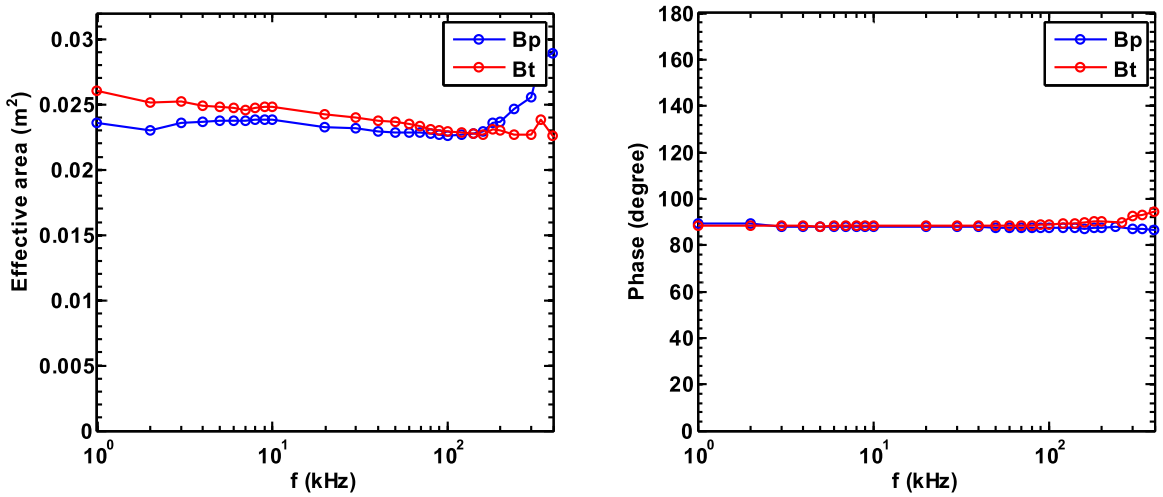

FIG. 6. Frequency response and phase test results of Bp and Bt magnetic probe. The phase shift is between the voltage of magnetic probe and the excitation current.

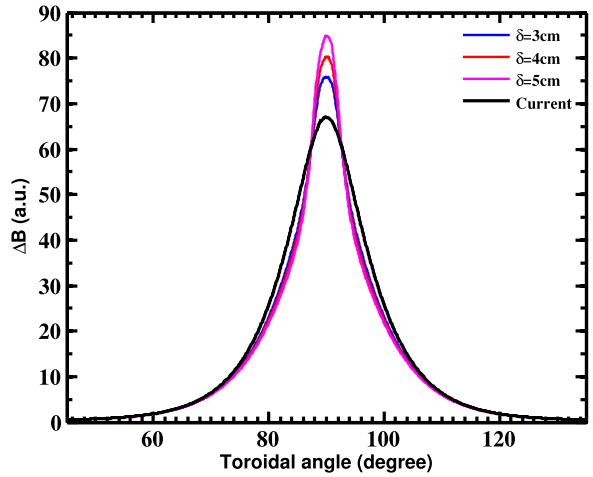

FIG. 7. Difference of magnetic fields varies with the distance between two probes δ. ΔB is normalized by μ_0 in order to compare with the current in the shell.

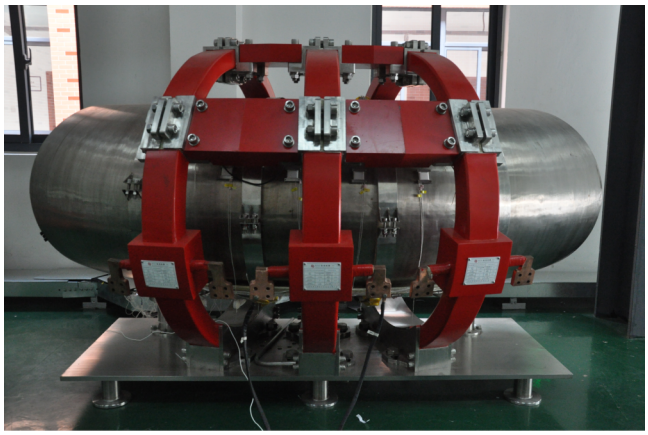

FIG. 8. Photo of the 1/4 vacuum vessel test bench whose structural size and materials are identical to the KTX device. Only three toroidal field coils are assembled with it.

Moreover, eddy currents obtained by differential operation have less noise than those from magnetic field signals. After filtering the common noise in the magnetic field signals, the eddy current has a larger SNR than the original signals.

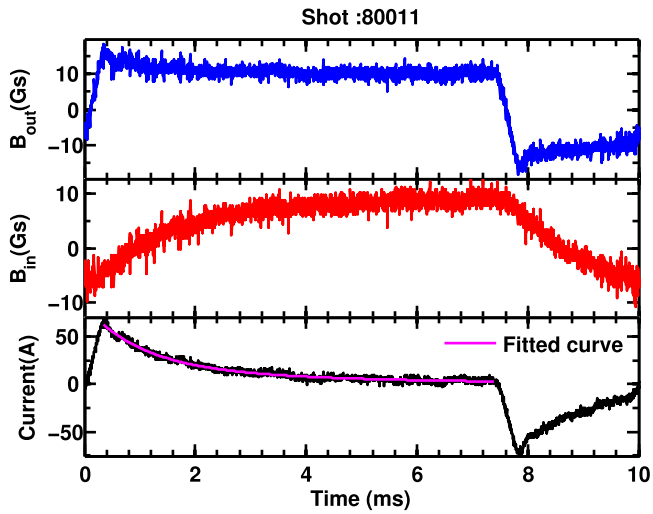

FIG. 9. Magnetic fields and eddy currents measured in the 1/4 vacuum vessel test bench.

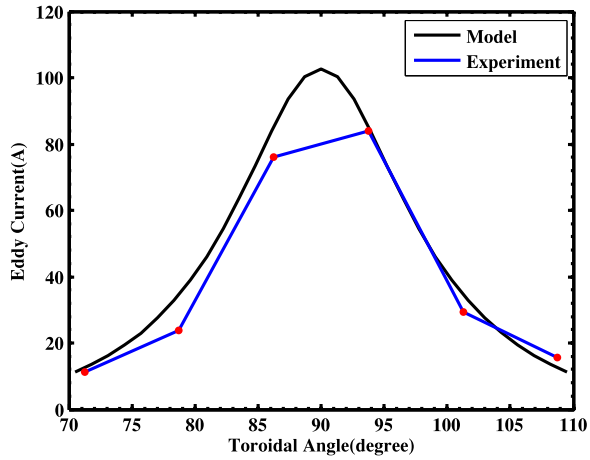

FIG. 10. Comparison of eddy currents from the bench test and model.

The middle of the six probes is at angle 90° (1/4 VV extends from 45° to 135°) and the angular interval of two probes is 7.5°. The peak values of the eddy current in the test are compared with the model in Fig. 10. The distribution of the

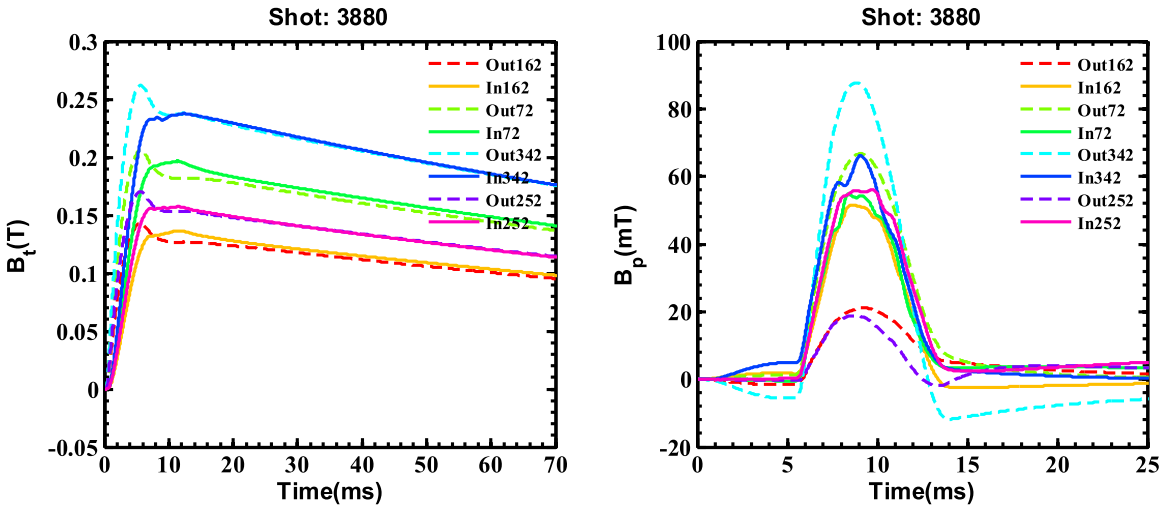

FIG. 11. Toroidal and poloidal fields measured by eddy current probe array in KTX. The magnetic fields of four poloidal angles are detected at a toroidal angle of 210°; the inner and outer magnetic fields are represented by solid lines and dashed lines.

poloidal eddy currents in the equatorial plane measured by the probes agrees well with the model prediction.

V. THE INITIAL RESULTS FROM KTX OPERATION

A. Eddy currents in the shell

The KTX was operating in the tokamak mode in shot No. 3880 and the toroidal field was applied at t = 0 ms. Results for the toroidal and poloidal fields detected by the eddy current probes are shown in Fig. 11. The magnetic fields of four poloidal angles are detected at a toroidal angle of 210°; the inner and outer magnetic fields are represented by solid lines and dashed lines. The toroidal field intensities decrease from top to bottom and are consistent with the position distribution of the magnetic probes, which are located at increasing major radius (decreasing toroidal field). The outer toroidal fields increase rapidly within 5 ms, followed by the inner fields; after peaking, both decay gradually. All toroidal fields at the four poloidal angles reach their peaks first, but the peaks of the inner fields are smaller than those of the outer fields.

The waveforms of the poloidal fields are clearly similar to the plasma current. There are significant differences between the outer poloidal fields, and the amplitude of the HFS poloidal field can be three times greater than that of the low field side. Also, their variation with time is much smoother than the inner fields. Between the inner poloidal fields, the differences are only as much as a factor of 1.3. Nevertheless, there are apparent disturbances seen in the Bp signals resulting from displacements and instabilities of the plasma in the VV during discharge. During the initial period 0-6 ms, when only the toroidal field is applied, poloidal fields oppose at poloidal

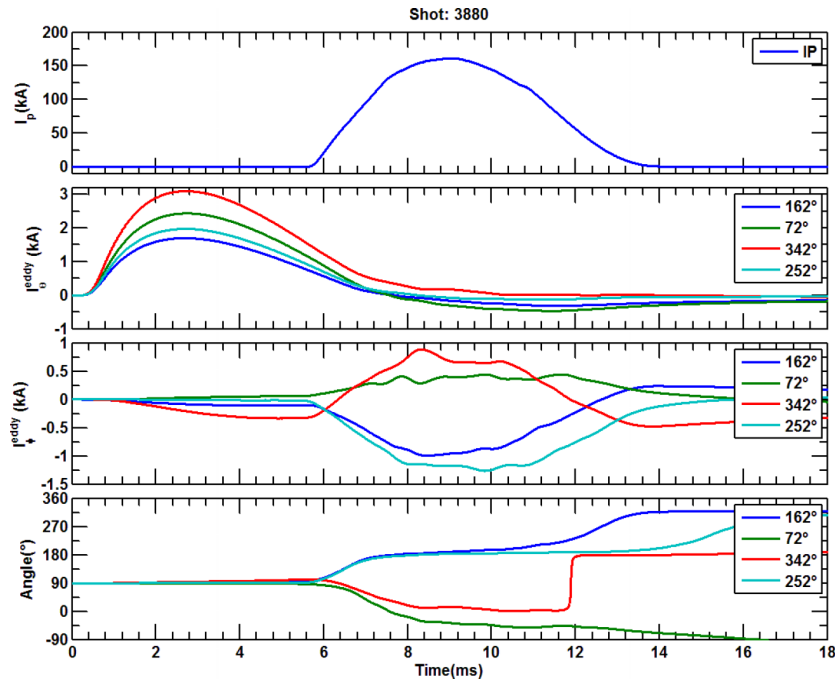

FIG. 12. *Ip*, amplitude, and angle of eddy currents measured by the ECPA in KTX (the angle range of 72° is −90° to 270° whereas others are 0°–360°).

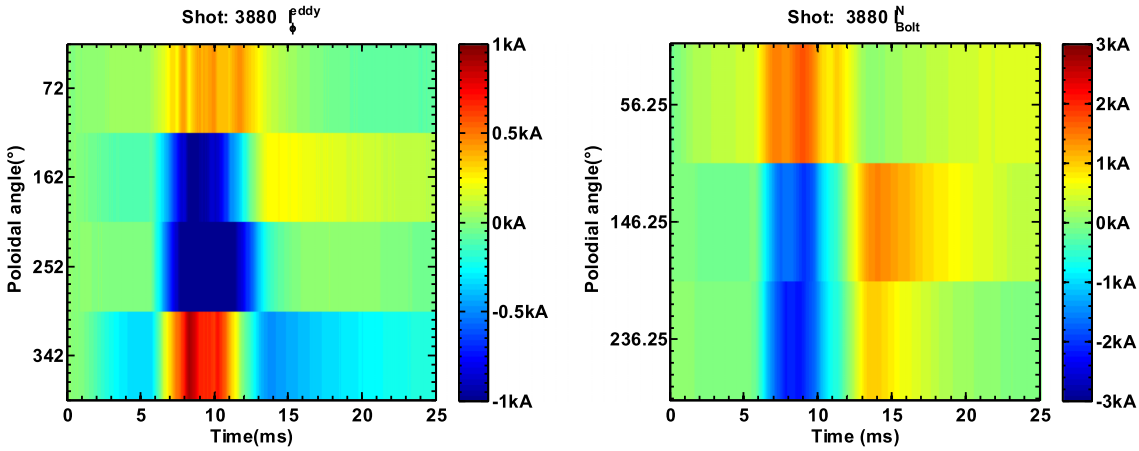

FIG. 13. Distribution of toroidal eddy currents and bolt currents at the gap shows a reasonable agreement in the poloidal direction; data at poloidal 326.25° are lacking.

angle 342° because of the existence of the toroidal gap at poloidal angle 0°. The poloidal eddy currents induced by the toroidal field coils have to flow along the toroidal direction at the gap, producing poloidal fields.

The plasma current, poloidal and toroidal eddy currents, and their angles for shot No. 3880 in the KTX (Fig. 12) show that the maximum plasma current is 160 kA and the discharge time is 6-13 ms. During the rising phase of the toroidal field, there are large poloidal eddy currents induced by the toroidal field coils in the shell and they have a similar 1/R distribution as the Bt because of the toroidal effect. The poloidal currents in the same direction peak with a maximum of 3 kA in 2.8 ms. At the same time, there is an obvious toroidal eddy current of about 0.3 kA, which is much less than the poloidal currents at poloidal angle 342° mentioned above. During the discharge, positive toroidal eddy currents at 72° and 342° and negative eddy currents at 162° and 252° flow in the shell, generating a magnetic field that pushes the plasma inward. The distribution of the toroidal eddy currents also shows that the plasma has an outward and downward shift.

Four eddy currents remain at 90° during the period 0-6 ms and move horizontally after 1.5 ms in the rising phase of the plasma current from the angular segment. The eddy currents at 162° and 252° turn to 180° indicating that they rotate anti-clockwise whereas the other two currents rotate clockwise to 0°. The four angles remain stable during plasma discharge while the eddy currents at 162° and 342° begin to reverse in the 0.8 ms before discharging end.

B. Eddy currents through copper bolts

Because of the engineering installation, not all the currents through the copper bolts have been obtained. For the three obtained (Fig. 13), their amplitudes are rather large indicating a strong inhibiting factor on the error fields. The zero crossing points of the bolt currents at about 12 ms are the same as the inversion points of the eddy current angles. The distribution of the toroidal eddy current and a fraction of the bolt currents on the gaps show a reasonable agreement in the poloidal direction. The amplitude of the bolt currents is almost fourfold that of the toroidal eddy current obtained by the magnetic probes, as the measurement coverage area for the former is just fourfold that of the latter.

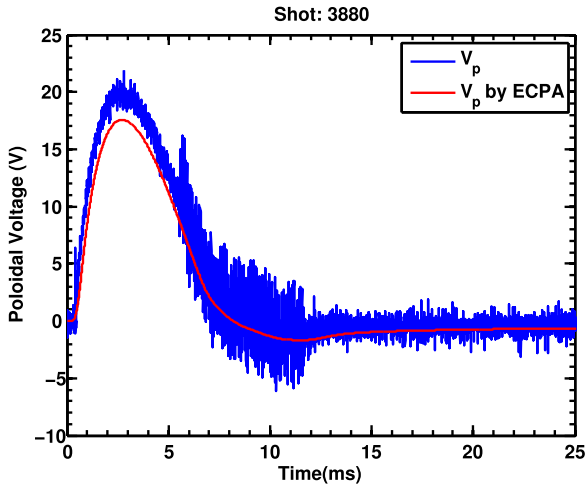

FIG. 14. Poloidal loop voltage obtained by a single loop coil and ECPA.

C. Electric field measurement

Aside from measurements of the magnetic field and eddy current, the vortex electric field also can be determined by the eddy current probe array. Because the eddy current in the shell is driven by the vortex electric field, it is easy to calculate the electric field based on Ohm's law. The poloidal loop voltage gained by the loop integral in the poloidal electric field is compared with the poloidal loop voltage measured by a single loop coil (Fig. 14). There is a very small difference between the two voltages being an indirect identification of the accuracy of the eddy current measurement. As the conductivity of the composite shell is rather high, the ECPA is very sensitive to the electric field and resolutions of 0.2 mV/cm are attainable.

VI. CONCLUSIONS

In RFP fusion devices, a conductive shell is always positioned around the edge of plasma. The passive eddy current in the shell contributes to maintaining plasma equilibrium and suppressing instabilities. An eddy current probe array, a

diagnostic tool to measure the eddy current in the composite shell, was introduced into the KTX. The spatial and temporal distribution of the eddy current in the shell is obtained by differential measurements of the 2D magnetic field and precise measurements of the currents passing through the copper bolts at the gaps.

The ECPA covers the area of the composite shell including the two poloidal gaps, providing a wide range of mode number detection. The non-uniform distribution of the 2D magnetic probes is helpful to resolve higher mode number. The measurable quantities obtained from ECPA include magnetic field B, eddy current I, and electric field E. It should be noted that both the amplitude and angle of the eddy current can be determined at each measurement point. Bench tests on a 1/4 VV bench demonstrate that the eddy current probes provide high quality signals with high SNRs. The preliminary results from the KTX show the probe array works as expected and the eddy current in the shell demonstrates that to date the plasma in the VV has an outward and downward shift. In future, ECPA will be applied to the feedback control to help regulate the active coils and improve plasma confinement.

ACKNOWLEDGMENTS

The authors express sincere thanks to all members of the KTX group. This work was supported by the Ministry of Science and Technology of China under Contract No. 2011GB106000 and the National Natural Science Foundation of China (Grant No. 11375193).

[1]A. Bondeson and D. J. Ward, Phys. Rev. Lett. **72**, 2709 (1994).
[2]T. C. Hender, C. G. Gimblett, and D. C. Robinson, Nucl. Fusion **29**, 1279 (1989).
[3]S. C. Guo and M. S. Chu, Phys. Plasmas **9**, 4685 (2002).
[4]F. Villone, Y. Q. Liu, R. Paccagnella, T. Bolzonella, and G. Rubinacci, Phys. Rev. Lett. **100**, 255005 (2008).
[5]D. A. Gates, J. E. Menard, and R. J. Marsala, Rev. Sci. Instrum. **75**, 5090 (2004).
[6]S. Tsaun and H. Jhang, Rev. Sci. Instrum. **77**, 016101 (2006).
[7]L. J. Liu, K. X. Yu, M. Zhang, G. Zhuang, X. Li, T. Yuan, B. Rao, and Q. Zhao, Rev. Sci. Instrum. **87**, 013501 (2016).
[8]L. Berzak, A. D. Jones, R. Kaita, T. Kozub, N. Logan, R. Majeski, J. Menard, and L. Zakharov, Rev. Sci. Instrum. **81**, 10E114 (2010).
[9]D. L. Chen, B. Shen, R. S. Granetz, Y. Sun, J. P. Qian, Y. Wang, and B. J. Xiao, Rev. Sci. Instrum. **86**, 103506 (2015).
[10]T. Bolzonella, N. Pomaro, G. Serianni, and D. Marcuzzi, Rev. Sci. Instrum. **74**, 1554 (2003).
[11]D. J. D. Hartog, J. T. Chapman, D. Craig, G. Fiksel, P. W. Fontana, S. C. Prager, and J. S. Sarff, Phys. Plasmas **6**, 1813 (1999).
[12]L. Marrelli *et al.*, Plasma Phys. Controlled Fusion **49**, B359 (2007).
[13]E. J. Strait, Rev. Sci. Instrum. **77**, 023502 (2006).
[14]P. V. Savrukhin and E. A. Shestakov, Rev. Sci. Instrum. **83**, 013505 (2012).
[15]Y. Ren, A. F. Almagri, G. Fiksel, S. C. Prager, J. S. Sarff, and P. Terry, Phys. Rev. Lett. **107**, 195002 (2011).
[16]W. Liu *et al.*, Plasma Phys. Controlled Fusion **56**, 094009 (2014).
[17]L. Bing *et al.*, Plasma Sci. Technol. **18**, 90 (2016).
[18]W. You *et al.*, Fusion Eng. Des. **108**, 28 (2016).